sustainability

Article

Monte Carlo Simulation and a Clustering Technique for Solving the Probabilistic Optimal Power Flow Problem for Hybrid Renewable Energy Systems

Mohamed S. Hashish [1], Hany M. Hasanien [1,*], Haoran Ji [2], Abdulaziz Alkuhayli [3], Mohammed Alharbi [3], Tlenshiyeva Akmaral [4], Rania A. Turky [5], Francisco Jurado [4] and Ahmed O. Badr [1]

1 Electrical Power and Machines Department, Faculty of Engineering, Ain Shams University, Cairo 11517, Egypt
2 The Key Laboratory of Smart Grid of Ministry of Education, Tianjin University, Tianjin 300072, China
3 Electrical Engineering Department, College of Engineering, King Saud University, Riyadh 11421, Saudi Arabia
4 Department of Electrical Engineering, University of Jaén, 23700 Linares, Spain
5 Electrical Engineering Department, Faculty of Engineering and Technology, Future University in Egypt, Cairo 11835, Egypt
* Correspondence: hanyhasanien@ieee.org

Abstract: This paper proposes a new, metaheuristic optimization technique, Artificial Gorilla Troops Optimization (GTO), for a hybrid power system with photovoltaic (PV) and wind energy (WE) sources, solving the probabilistic optimum power flow (POPF) issue. First, the selected algorithm is developed and evaluated such that it applies to solve the classical optimum power flow (OPF) approach with the total fuel cost as the objective function. Second, the proposed algorithm is used for solving the POPF, including the PV and WE sources, considering the uncertainty of these renewable energy sources (RESs). The performance of the suggested algorithm was confirmed using the standard test systems IEEE 30-bus and 118-bus. Different scenarios involving different sets of the PV and WE sources and fixed and variable loads were considered in this study. The comparison of the obtained results from the suggested algorithm with other algorithms mentioned in this literature has confirmed the efficiency and performance of the proposed algorithm for providing optimal solutions for a hybrid power system. Furthermore, the results showed that the penetration of the PV and WE sources in the system significantly reduces the total cost of the system.

Keywords: probabilistic optimal power flow; renewable energy sources; uncertainties; Monte Carlo Simulation; K-means clustering; Elbow method

check for updates

Citation: Hashish, M.S.; Hasanien, H.M.; Ji, H.; Alkuhayli, A.; Alharbi, M.; Akmaral, T.; Turky, R.A.; Jurado, F.; Badr, A.O. Monte Carlo Simulation and a Clustering Technique for Solving the Probabilistic Optimal Power Flow Problem for Hybrid Renewable Energy Systems. *Sustainability* **2023**, *15*, 783. https://doi.org/10.3390/su15010783

Academic Editors: Reza Daneshazarian and Shahrzad Soudian

Received: 14 November 2022
Revised: 24 December 2022
Accepted: 27 December 2022
Published: 1 January 2023

1. Introduction

The OPF is still a significant subject in the community of power-system researchers since it began almost half a century ago. The OPF is considered a nonlinear, multi-dimensional, and large-scale problem in the operation of power systems. The primary purpose of the OPF is to optimize a particular objective function by meeting a group of operational and physical restrictions mandated by equipment and power system restrictions. The objective function can be divided into single- and multi-objective functions. Examples of objective functions include the fuel costs for generators, their emission rates, the electricity grid's losses, and the security index of the voltage. Equality and inequality constraints involve power-balance equations and limitations on all state and control variables. The control variables involve the active power of the generator, the bus voltage of the generator, the transformer tap ratios, and the VAR (volt–ampere reactive) compensators, whereas the state variables include the reactive power outputs from the generators, the bus load voltages, and the network line flow. Consequently, the electric utilities use the OPF issue as an essential tool to describe secure and economically advantageous operational conditions for power systems.

The earliest OPF problem was solved using traditional mathematical programming techniques, successfully proving their viability [1]. Conventional methods of optimization are used for solving the OPF problem, such as the method of Newton [1], the method of gradient projection [2], the method of linear programming [3], and the method of interior point [4]. The conventional optimization methods are accompanied by many difficulties reported in [5]. Due to the continuously developing optimization issues, several techniques have been established to solve the OPF; artificial intelligence techniques and meta-heuristic, search-based optimization methods have been developed for solving the OPF issue. Search-based optimization methods have been recently used for solving the OPF problem, such as the particle swarm optimizing algorithm (PSO) [6,7], genetic algorithms method (GA) [8], enhanced genetic algorithms method [9], differential evolution algorithm method [10,11], gravitational searching algorithm method (GSA) [12,13], improving colliding bodies algorithm [14], multi-phase searching optimization algorithm [15,16], improved PSO [17], fuzzy-based hybrid PSO approach [18], biogeography-based optimizing algorithm [19], black-hole optimization algorithm [20], harmony search optimization algorithm [21], imperialist competitive optimization algorithm [22], grey wolf optimization [23], PSO hybrid with GSA algorithm [24], and the bee colony optimization algorithm [25]. Several multi-objective functions for the OPF problem were introduced in [11,17,18,23].

Currently, there is an increase on the grid in the use of RESs such as solar and wind energy [26,27]. Although RESs have benefits such as lowering pollution and saving resources, the consequent rise in load uncertainty and associated uncertainty in power production have created new difficulties in the operation and distribution of power networks. To successfully integrate those sources into the grid and provide a secure and lucrative power market, it is critical to manage them properly [26,28]. Therefore, their stochastic nature must be considered while integrating these sporadic RESs into the grid. Solving the OPF problem has been significantly difficult because of the uncertainties of the added RESs to the system. Furthermore, solving the OPF is computationally intensive and impractical because it necessitates running numerous simulations to consider most of the possible operating conditions. Both traditional and intelligence-based techniques (deterministic techniques) for solving the OPF issue have been mentioned in the previous paragraph. Still, the probabilistic techniques must be considered to address the uncertainty of the RESs.

Probabilistic techniques can offer improved solutions and appropriate accuracy when considering uncertainties [29,30]. Therefore, it is preferred that the POPF problem is solved using a probabilistic approach rather than the deterministic point of view, as thoroughly reviewed by Ramadhani et al. in [31] and Prusty and Jena in [32,33]. In power systems with numerous PV and wind units, many probabilistic techniques are used in solving the OPF issue. To obtain the PDF of the PV system's output power, the two-point estimate method (2PEM), dependent on the moments' technique, was introduced in [34]. However, the moments' method sometimes produces estimates which do not fall within the parameter space, resulting in the solution becoming unreliable. The Cornish–Fisher expansion was presented in [35] to handle the uncertainties of the PV sources Still, this method does not produce accurate estimations when handling problems that contain non-continuous return functions and complex structures [36]. A POPF problem with wind power inserted into the system was presented in [37], and the heuristic approach was used to calculate the PDF of the wind speed. However, real data must be available to calculate the PDF accurately. The kernel-density estimation technique estimated the wind speed probability distribution [38]. However, this approach is impractical since the density estimate depends on where the bins are when they are initially placed. The number of bins increases exponentially as the number of dimensions increases. According to the Latin hypercube random sampling technique, the mean–variance skewness methodology for stochastic and nonconvex OPF incorporating wind energy was developed in [39]. However, this approach is hampered by the sample points' statistical dependencies, and it does not appear to be noticeably better than other random sample methods for sensitive analysis. To obtain the PDF of the power produced from a wind energy system, the Monte Carlo Simulation (MCS) and its variations were taken into consideration in [40,41]. The MCS technique was used to develop an OPF issue for a power system with PV and WE units [42].

This study formulates and solves the POPF issue with a hybrid power system that contains wind and solar energy sources. These are the primary contributions made in this paper:

1. Implement and solve the POPF approach while allowing RESs to become more integrated into the electricity grid using Artificial Gorilla Troops Optimization (GTO).
2. Obtain actual historical data for the summers of four years (2018, 2019, 2020, and 2021). The whole data are used to mimic a more accurate 24-h summer day and provide curve-fitting for each hour of data for PV and wind using the Beta and Weibull PDFs, respectively.
3. Combine the MCS with the K-means clustering method to reduce the significant computational time.
4. Apply the Elbow method to the K-means clustering method to find the optimal initial number of clusters and reduce the computational time.
5. Solve the POPF for a variable load of a weekend day in summer using the GTO.

The following portions of this paper are arranged: Section 2 presents the problem formulation, the POPF, and its restrictions and penalty terms. Section 3 introduces the mathematical models of the RESs. The Monte Carlo Simulation method combined with the K-means clustering method and the Elbow method is introduced in Section 4. Section 5 offers the Artificial Gorilla Troops optimization algorithm. The simulation results from the suggested optimization technique applied to the standard IEEE 30- and 118-bus systems are shown in Section 6, along with a comparison study on several optimization techniques reported in this paper. Finally, Section 7 concludes the whole study.

2. Problem Formulation

In this study, the proposed GTO method is applied to solve the classical OPF problem with its objective function implemented to reduce the generation cost. To solve the POPF, the algorithm's structure is modified to include the uncertainty and stochastic nature of RESs and the variable load profiles. The following equations provide a formulation for the OPF problem:

$$\text{Minimize}: \ f(q,w) = f_1(q,w), f_2(q,w), \ldots.., f_{N_{obj}} \tag{1}$$

$$\text{Subject to}: \ \mathrm{g}\,(q,w) = 0 \tag{2}$$

$$h(q,w) \ \leq \ 0 \tag{3}$$

where q is the state variable, w denotes the control variable, $f(q,w)$ denotes the objective function, $h\,(q,w)$ denotes the inequality constraints and $\mathrm{g}\,(q,w)$ denotes the equality constraints.

2.1. Objective Function

The OPF issue in this study is to reduce the total fuel cost of conventional generators. An equation formulates the cost function in the quadratic form of the real power generated. The cost function can be mathematically formulated in Equations (4) and (5).

$$\text{Minimize} \ F = \sum_{h=1}^{24}\sum_{j=1}^{NG} C_{j,h}\left(P_{Gj,h}\right) \tag{4}$$

$$C_{j,h}\left(P_{Gj,h}\right) = a_j \ P^2_{Gj,h} + b_j P_{Gi,h} + c_i \tag{5}$$

where F represents the objective function, $P_{Gj,h}$ denotes the power generated at bus 'j' at hour 'h', and NG represents the total number of conventional generators. The objective function is recomputed for each hour to obtain the optimal generation cost hourly.

2.2. Equality Constraints

The power-balance equation imposes equality constraints by requiring that active and reactive power generated must match the load demand and power losses. The equality constraints consist of a group of nonlinear power-flow equations that can be formulated in Equations (6) and (7).

$$\mathrm{P}_{Gi} - \mathrm{P}_{Di} = V_i \sum_{j=1}^{NB} V_j \left[G_{\mathrm{ij}} cos\left(\delta_{\mathrm{ij}}\right) + B_{\mathrm{ij}} sin\left(\delta_{\mathrm{ij}}\right) \right] \, \forall \, \mathrm{i} \in \mathrm{NB} \tag{6}$$

$$\mathrm{Q}_{Gi} - \mathrm{Q}_{Di} = V_i \sum_{j=1}^{NB} V_j \left[G_{\mathrm{ij}} sin\left(\delta_{\mathrm{ij}}\right) - B_{\mathrm{ij}} \ os\left(\delta_{\mathrm{ij}}\right) \right] \, \forall \, \mathrm{i} \in \mathrm{NB} \tag{7}$$

where P_{Gi} and Q_{Gi} represent the generation's active and reactive power of the bus i, respectively. P_{Di} and Q_{Di} represent the load demand's active and reactive power, respectively. NB denotes the total number of buses, G_{ij} denotes the transfer conductance between i and j buses, and B_{ij} denotes the susceptance between i and j buses. The $= \delta_i - \delta_j$. Finally, V_i and V_j are the voltages of bus i and bus j, respectively.

2.3. Inequality Constraints

The inequality constraints are imposed by the operating restrictions on the power system's equipment and the security limitations on the lines and load buses.

- Generator constraints:

$$P_{TGi}^{min} \leq P_{TGi} \leq P_{TGi}^{max}, \quad i = 1, \ldots, \mathrm{NG} \tag{8}$$

$$Q_{TGi}^{min} \leq Q_{TGi} \leq Q_{TGi}^{max}, \quad i = 1, \ldots, \mathrm{NG} \tag{9}$$

$$V_{Gi}^{min} \leq V_{Gi} \leq V_{Gi}^{max}, \quad i = 1, \ldots, \mathrm{NG} \tag{10}$$

- Security constraints:

$$V_{L_p}^{min} \leq V_{L_p} \leq V_{L_p}^{max}, \quad p = 1, \ldots, \mathrm{NPQ} \tag{11}$$

$$S_{l_q} \leq S_{l_q}^{max}, \qquad q = 1, \ldots, \ \mathrm{NTL} \tag{12}$$

Equation (8) represents the thermal generator's active power boundaries. Equation (9) represents the thermal generator's reactive power capabilities. NG denotes the total number of thermal generators. Equation (10) represents the limits of voltage on generator buses (PV buses), while Equation (11) represents the limits of voltage on load buses (PQ buses). Equation (12) represents the capacity of the transmission line. NTL and NPQ denotes the number of lines and load buses in the network, respectively.

It is noteworthy that the active and reactive power equations' equality constraints are automatically met when the power-flow problem is converted into a solution. The inequality constraints, such as the active power and the bus voltage of the generator (except for slack, which is regarded as linked to bus 1), are the control variables. The optimization algorithm selects possible values for such control variables, which are bounded by their limits. The other inequality constraints, such as the power of the slack generator, voltage limits of the load bus, reactive power output from the remaining generators, and the capacity of the transmission lines, require special considerations such that their values must not exceed the limits. Therefore, the objective function incorporates these inequality constraints as quadratic penalty factors. Accordingly, the new objective function is given in Equation (13) [43].

$$F = \left[F_{\mathrm{C}} + \lambda_{\mathrm{P}} \left(P_{\mathrm{TG1}} - P_{\mathrm{TG1}}^{lim} \right)^2 + \lambda_{\mathrm{V}} \sum_{i=1}^{\mathrm{NPQ}} \left(V_{\mathrm{Li}} - V_{\mathrm{Li}}^{lim} \right)^2 + \lambda_{\mathrm{Q}} \sum_{i=1}^{\mathrm{NG}} \left(Q_{\mathrm{TG}i} - Q_{\mathrm{TG}i}^{lim} \right)^2 + \lambda_{\mathrm{S}} \sum_{i=1}^{\mathrm{NTL}} \left(S_{\mathrm{li}} - S_{\mathrm{li}}^{lim} \right)^2 \ldots \right]_{n \times 1} \tag{13}$$

where λ_P, λ_V, λ_Q, and λ_S represent penalty factors. The chosen values for all penalty factors are $\lambda_P = 100,000,000$, $\lambda_V = \lambda_Q = 50,000$, and $\lambda_S = 1000$.

3. Mathematical Modeling of the RES

The primary generation elements in the power system are wind, solar, and thermal generators. Therefore, solar and wind power are considered in solving the POPF problem [44]. However, due to the uncertain nature of the RESs (as mentioned earlier), the generation power from the RESs incorporates high uncertainties [45,46]. Consequently, it is crucial to precisely simulate the PV and WT generators in the manners described below.

3.1. Modeling the WE Power Generation

The wind speed variations are described using the Weibull PDF [36,47]. The probability of wind speed v (m/s) may be expressed as follows using Weibull PDF:

$$f(v) = \left(\frac{k}{c}\right)\left(\frac{v}{c}\right)^{(k-1)} \exp\left[-\left(\frac{v}{c}\right)^{k}\right], \qquad v \geq 0 \tag{14}$$

where c and k denote the Weibull distribution's scale and shape factors, respectively. By using the stochastic variable wind speed, the power output from wind generators is determined as follows:

$$P_w(v) = \begin{cases} 0 & v < v_{in} \text{ Or } v \geq v_{out} \\ P_{wr}\frac{v - v_{in}}{v_r - v_{in}} & v_{in} \leq v < v_r \\ P_{wr} & v_{in} \leq v < v_r \end{cases} \tag{15}$$

where v, and v_r represent current and rated wind speed, respectively, P_{wr} represents rated output power, and v_{in} and v_{out} represent cut-in and cut-out speed, respectively. The data obtained for wind speed was at the height of 33 ft (10 m). However, according to the Enercon E82-E4 product datasheet, a 3-MW wind turbine's hub height is generally 84 m, so to obtain wind speed at that height, the method of Weibull wind speed distribution extrapolation is applied, which can be formulated as follows [48]:

$$C_2 = C_1\left(\frac{h2}{h1}\right)^{n} \tag{16}$$

$$k_2 = k_1\frac{1 - 0.0881\ln\left(\frac{h_1}{hr}\right)}{1 - 0.0881\ln\left(\frac{h_2}{hr}\right)} \tag{17}$$

where hr is a 10 m reference height and n is a power. The following formula may be used to find the power n:

$$n = \frac{0.37 - 0.0881\ln(C_1)}{1 - 0.0881\ln\left(\frac{h_1}{hr}\right)} \tag{18}$$

Figure 1 shows the Weibull PDF for the wind speed data over the equivalent 24-h day in summer. Table 1 shows the parameter of the Weibull PDF for the equivalent 24-h summer day of the real-time historical date such that the Weibull parameters are scale parameters (C) and shape parameters (K).

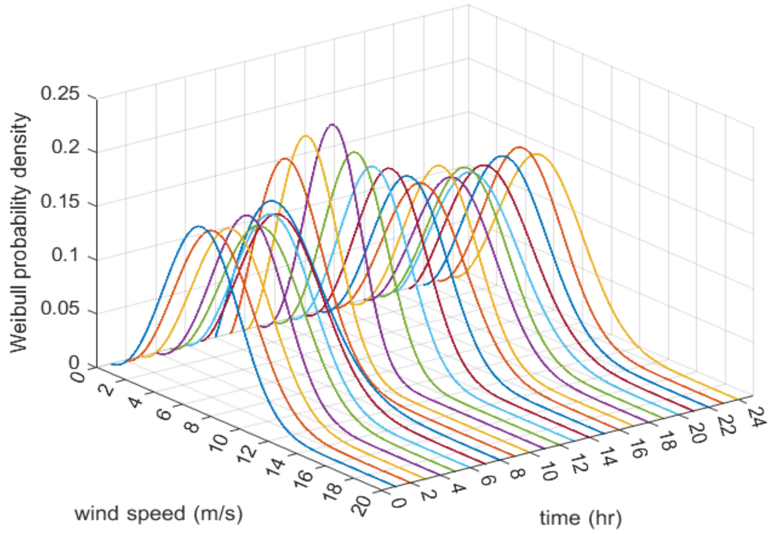

Figure 1. Weibull PDF of the wind data for the summer season.

Table 1. The Weibull parameters of the equivalent 24-h summer day for wind data.

Hour	C	K	Hour	C	K
1	7.274	3.043	13	6.793	3.036
2	7.257	2.854	14	6.968	3.036
3	7.417	2.921	15	7.288	2.998
4	7.444	3.146	16	7.372	2.806
5	7.504	2.862	17	7.357	3.102
6	7.214	2.858	18	7.456	2.821
7	6.852	2.547	19	7.278	2.845
8	5.843	2.072	20	7.008	2.475
9	5.127	2.309	21	6.887	2.475
10	5.208	2.678	22	6.949	2.638
11	5.793	3.232	23	6.984	2.771
12	6.439	3.149	24	7.279	2.716

3.2. Modeling the PV Power Generation

Solar irradiance is very uncertain as it changes depending on several variables such as the time of day, month, season, weather, and the direction in which the solar generator faces the sun. According to the Beta PDF [36,49], the probability distribution for solar irradiation is as follows:

$$f(R) = \frac{\Gamma(\alpha+\beta)}{\Gamma(\alpha)\Gamma(\beta)} R^{a-1}(1-R)^{\beta} \tag{19}$$

where $f(R)$ is the Beta PDF of solar radiation. The incomplete gamma function is represented by $\Gamma(.)$. R represents the solar radiation [W/m^2]. By using the stochastic variable solar irradiance, the output power of solar generators is determined as follows:

$$P_{pv}(R) = \begin{cases} P_{pv,r}\left(\frac{R^2}{RCR_{STD}}\right) & 0 \leq R \leq R_C \\ P_{pv,r}\left(\frac{R}{R_{STD}}\right) & R_C \leq R \leq R_{STD} \\ P_{pv,r} & R_{STD} \leq R \end{cases} \tag{20}$$

where R_C represents a certain radiation point and R_{STD} represents solar radiation within standard conditions. Figure 2 shows the Beta PDF for the solar irradiance data over the equivalent 24-h day in summer. Table 2 shows the parameter of the Beta PDF for the equivalent 24-h summer day of the real-time historical date such that the Beta parameters are shape parameter 1 (α) and shape parameter 2 (β).

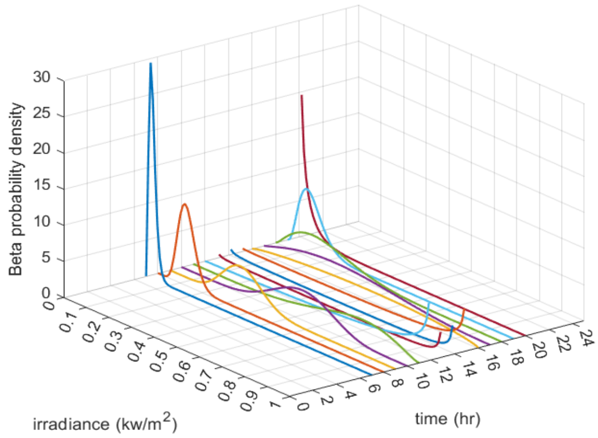

Figure 2. Beta PDF of the PV data for the summer season.

Table 2. The Beta parameters of the equivalent 24-h summer day for the PV data.

Hour	α	β	Hour	α	β
1	0	0	13	0.412	0.044
2	0	0	14	0.372	0.055
3	0	0	15	0.928	0.426
4	0	0	16	1.726	1.639
5	0	0	17	2.185	3.603
6	0	0	18	2.367	7.990
7	3.540	119.773	19	3.837	31.290
8	10.900	74.130	20	0.534	17.101
9	10.497	21.772	21	0	0
10	8.670	7.613	22	0	0
11	5.887	2.629	23	0	0
12	2.159	0.496	24	0	0

In this paper, the wind turbine parameters were v_{in} = 3 m/s, $v_{out} = 25\frac{\text{m}}{\text{s}}$, and $v_r = 16$ m/s. The rated power output for each turbine was P_{wr} 3 MW; this value is presented in the Enercon E82-E4 product datasheet. For the PV generator, R_C was set to be 120 W/m^2 and the R_{STD} was set to be 1000 W/m^2. Real-time historical data was used for solar irradiance and wind speed. These data weres for the summer seasons of four years (2018, 2019, 2020, and 2021). The real-time historical data is presented in [50]. Whole data were used to mimic a more accurate 24-h summer day such that the curve fitting, either by Weibull or Beta PDF, was performed for each hour of that day.

4. Monte Carlo Simulation Combined with K-Means Clustering and Elbow Method

As was mentioned in the previous sections, the summer data for the last four years was represented by an equivalent 24-h day, and curve fitting was applied for each hour. For each hour there was a vast number of operating conditions that needed to be taken into consideration. Therefore, MCS was run for 8000 scenarios for each hour of these data and were used in the analysis. The MCS was then combined with K-means clustering and the Elbow method, as is presented in the following subsections.

4.1. Monte Carlo Simulation

To integrate the PV and WE sources into the power system, the power system must deal with all possible scenarios due to the uncertain nature of renewable energy. Accordingly, it is essential to use a stochastic technique instead of the deterministic one. A Monte Carlo Simulation (MCS) was used in this research study. It is also known as multiple probability simulation for the stochastic technique. MCS is a probabilistic simulation technique to estimate the possible outcomes for uncertain situations. It can also be used to obtain stochastic outcomes from random variables [51]. The MCS was chosen because it is the most suitable technique for large, complex systems with a high number of uncertainties [36]. After making curve fitting for each hour of the data over the equivalent summer day, the MCS was run with 8000 scenarios for each hour. Consequently, there were a lot of scenarios overall, and many iterations were required, so a clustering technique was used in this paper to reduce the substantial computational time. Figures 3 and 4 show two examples of wind speed distribution and solar irradiance after running the MCS for 8000 scenarios for hour 10 with their scale and shape parameters.

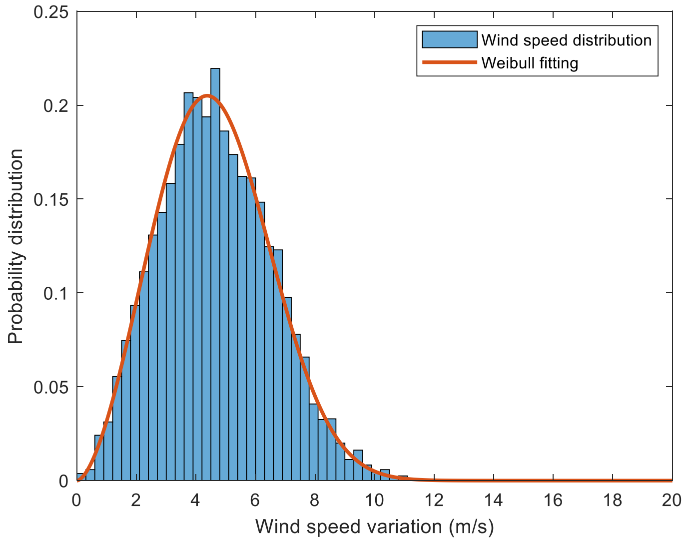

Figure 3. Wind speed variation in (m/s) for hour 10 (c = 5.2076, k = 2.6783).

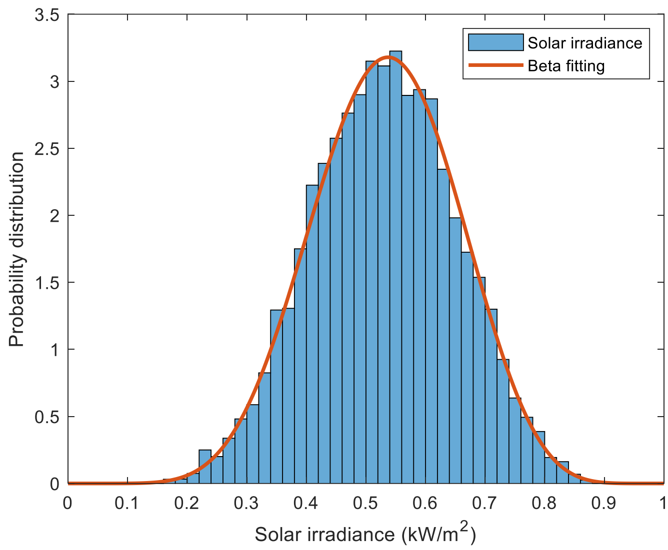

Figure 4. Solar irradiance in (kW/m^2) at hour 10 (α = 8.67, β = 7.6126).

4.2. K-Means Clustering

The MCS was combined with the K-means clustering method to reduce the overall number of scenarios and iterations [52]. K-means clustering is a partitioning clustering method in which the data points are sectionized into different sets (clusters), mentioned by the number K, in which each cluster depends on how similar the data points are [53] and is considered as an iterative algorithm within the initial number of clusters K, which must be manually determined by the user [54]. K-means clustering is performed in two steps:

1. Determine the best centroids or center points—K values—using an iterative process.
2. Set each data point to the closest K-center.

Figures 5 and 6 show an example of the data for wind speed and solar irradiance at hour 19, the initial centroid points, the final locations of the centroids after 100 iterations, and each set of data belongs to each centroid, as during iteration the centroids' location is changed to reach the best location. The trial-and-error method is used to determine the best number of iterations such that after 100 iterations the location of the centroids is not changed anymore.

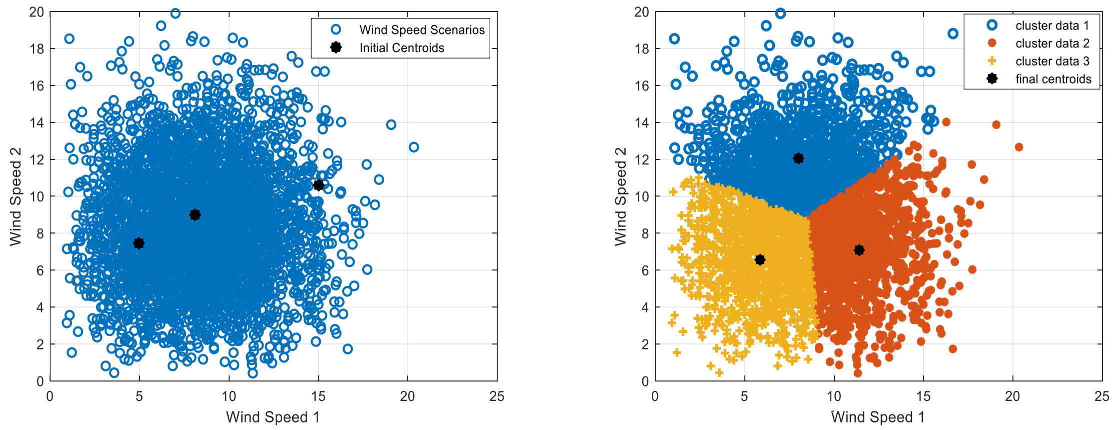

(**a**) (**b**)

Figure 5. Example of wind speed data at hour 19 after running the MCS for 8000 scenarios: (**a**) the initial centroid points and (**b**) the final locations of the centroids, and each set of data belonging to each centroid.

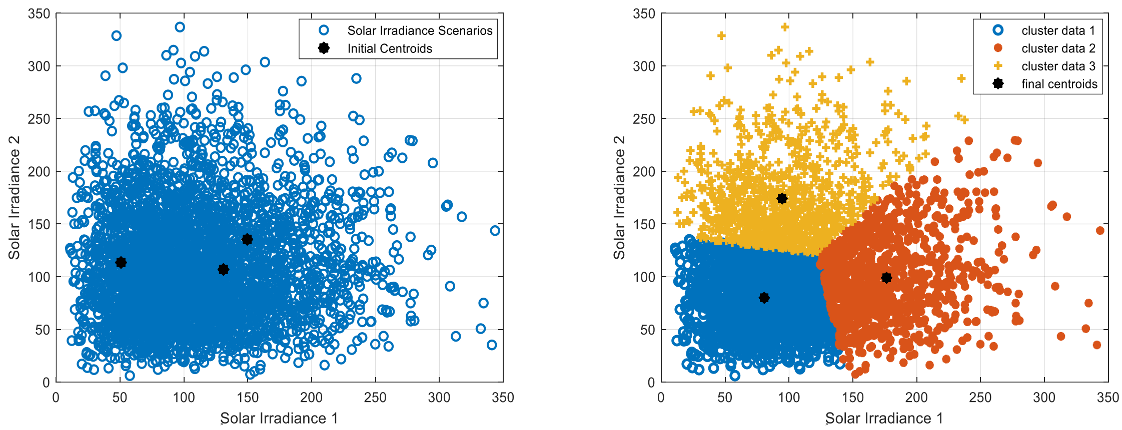

(**a**) (**b**)

Figure 6. Example of the data ofor solar irradiance at hour 19 after running the MCS for 8000 scenarios: (**a**) the initial centroid points and (**b**) the final locations of the centroids, and each set of data belonging to each centroid.

4.3. Elbow Method

The main weakness of the K-Means Clustering method is that it randomly assumes the number of clusters. Therefore, a cluster optimization technique is required to obtain the optimal number of clusters. [54]. The Elbow method determines the best number of clusters such that K-means clustering is run for the data set with assumed clusters. The sum of square error (SSE) is calculated for each assumed number of clusters, and the most significant difference from the angle of the elbow (knee point) shows the best number of clusters [55]. Initially, it is assumed that there are between one to ten clusters, and then, for each number of clusters Elbow method is applied, an SSE is calculated. The calculations showed that the angle of the elbow (the most significant difference) is formed when three clusters are used. Accordingly, the optimal number of clusters is K = 3. From both Figures 7 and 8, it is clear that the optimum number of clusters is three.

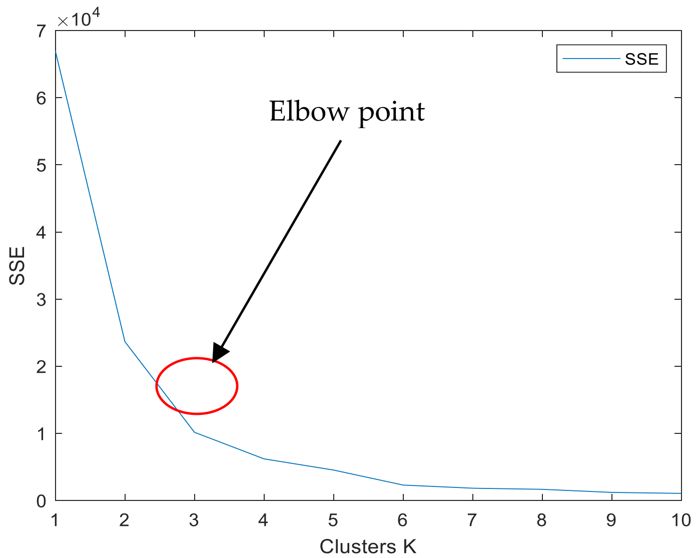

Figure 7. SSE for wind speed data with the number of clusters at hour 14.

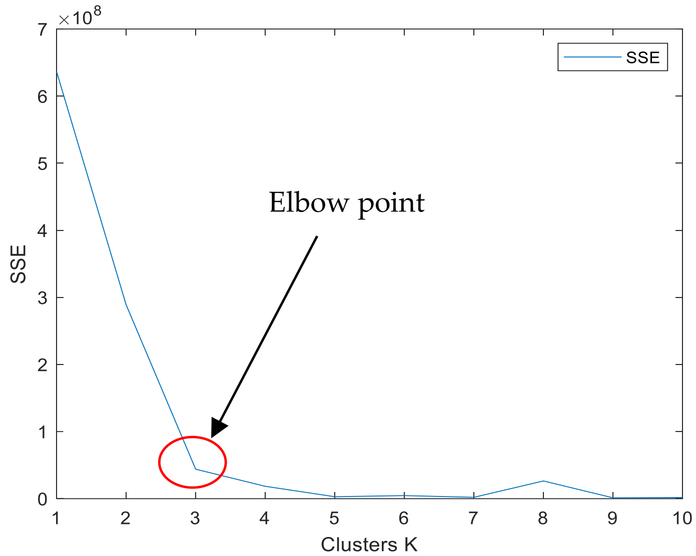

Figure 8. SSE for solar irradiance data with the number of clusters at hour 14.

5. Proposed Method

The GTO technique was selected to solve the POPF problem for different scenarios. The GTO is a nature-inspired metaheuristics algorithm inspired by the gorilla troop's social intelligence in nature [56]. Figure 9 presents the GTO flowchart for easier comprehension, and each step's formulation algorithm is fully described in detail. The following mechanisms are a description of the many processes that the GTO algorithm employs for optimization tasks.

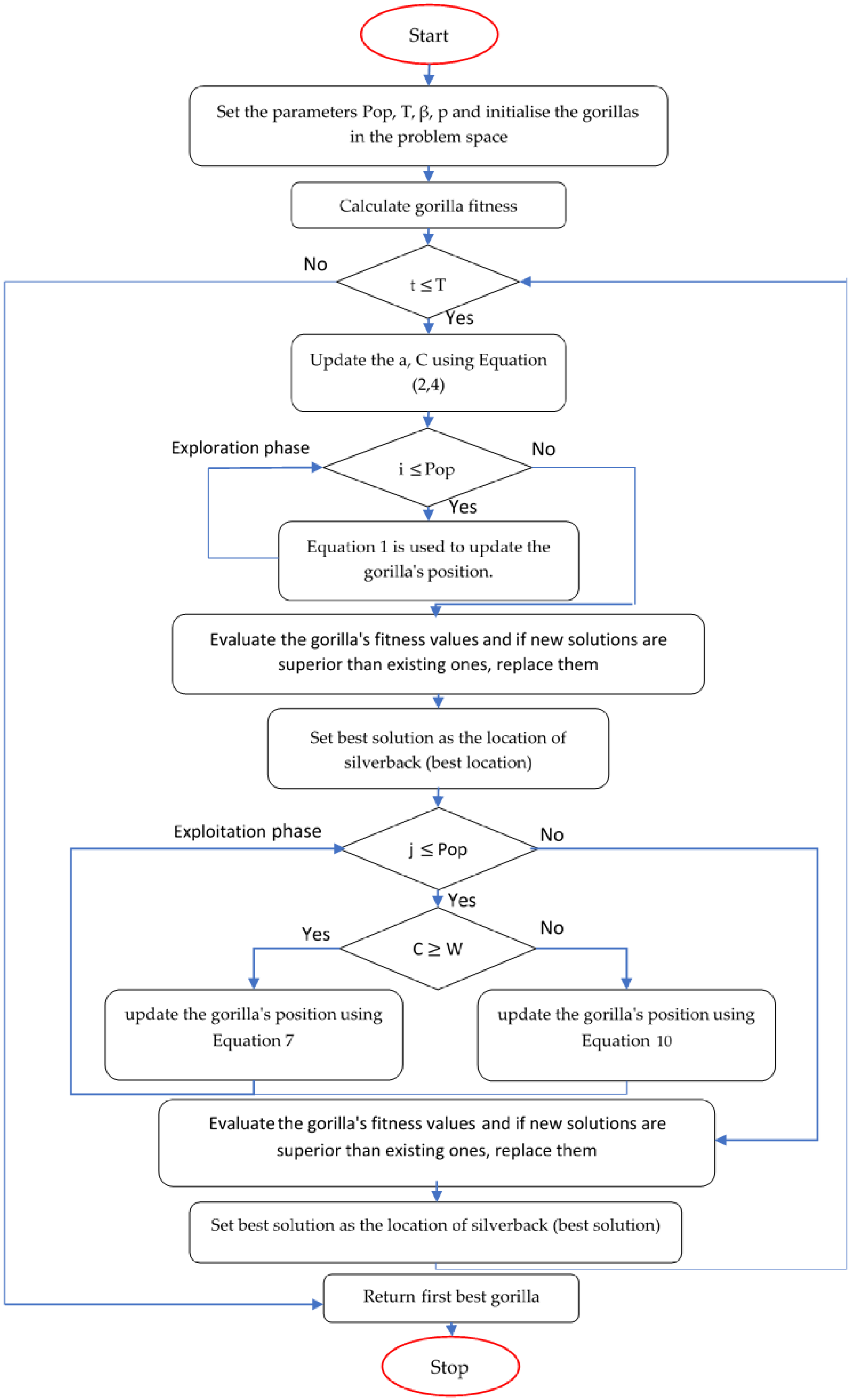

Figure 9. Flowchart of the Gorilla Troops Optimizer [56].

5.1. Exploration Phase

The exploration phase involves three primary mechanisms, which are: moving to other gorillas where this mechanism is selected when rand ≥ 0.5, migrating to an unknown location where this mechanism is selected when rand $\leq p$, and migrating in the direction of a known location where this mechanism is selected when rand < 0.5. Each of these three techniques is chosen based on a standard process. Where p is a parameter used to select the mechanism of migrating to an unknown location, each of these mechanisms presents a great ability of the GTO technique. The following equations simulate the three mechanisms utilized in the exploration stage [56].

$$GX(t+1) = \begin{cases} (UB - LB) \times r_1 + LB, & \text{rand} < p \\ (r_2 - C) \times X_r(t) + L \times H, & \text{rand} \geq 0.5 \\ X(i) - L \times (L \times (X(t) - GX_r(t)) + r_3 \times (X(t) - GX_r(t))), & \text{rand} < 0.5 \end{cases} \tag{21}$$

$$C = F \times \left(1 - \frac{It}{MaxIt}\right) \tag{22}$$

$$F = \cos(2 \times r_4) + 1 \tag{23}$$

$$L = C \times l. \tag{24}$$

$$H = Z \times X(t) \tag{25}$$

$$Z = [-C, C] \tag{26}$$

5.2. Exploitation Phase

The exploitation phase includes two behaviors: following the silverback and competing with adult females. It is possible to choose between them using the value of C calculated in Equation (22). Following the silverback method is chosen if $C \geq W$. This behavior can be modeled as follows:

$$GX(t+1) = L \times M \times (X(t) - X_{\text{silverback}}) + X(t) \tag{27}$$

$$M = \left(\left|\frac{1}{N}\sum_{i=1}^{N} GX_i(t)\right|^{g}\right)^{\frac{1}{g}} \tag{28}$$

$$g = 2^L \tag{29}$$

However, if $C < W$, the competition with adult females is selected. After some time, when adolescent gorillas reach puberty, they eventually engage in violent competition with other male gorillas in their group for the attention of adult females. This behavior is simulated as follows:

$$GX(i) = X_{\text{silverback}} - (X_{\text{silverback}} \times Q - X(t) \times Q) \times A \tag{30}$$

$$Q = 2 \times r_5 - 1 \tag{31}$$

$$A = \beta \times E, \tag{32}$$

$$E = \begin{cases} N_1, & \text{rand} \geq 0.5 \\ N_2, & \text{rand} < 0.5 \end{cases} \tag{33}$$

At the end of the exploitation phase, the cost of each GX solution is assessed, and if the cost of $GX\ (t)$ is less than the cost of $X\ (t)$, the $GX\ (t)$ solution is adopted as the $X\ (t)$ solution. The silverback is considered the best solution found throughout the whole population.

6. Simulation Results and Discussion

This paper proposed a solution for the OPF and POPF issues by applying the GTO algorithm. To verify the viability and performance of the suggested GTO-based OPF and POPF problem, the IEEE 30-bus and 118-bus systems were applied. Table 3 lists the details of these two power systems [36]. The effectiveness of the suggested algorithm is compared with GA (Genetic Algorithm) [57], PSO (Particle Swarm Optimization) [58], SFO (Sunflower Optimization) [59], HHO (Novel Harris Hawk Optimization) [60], and HFPSO (Hybrid Firefly Particle Swarm Optimization) [61] for a classical OPF. Algorithms used as competitors were the HHO and SFO for the POPF, including renewable energy. The control parameter of the OPF issue wasre the active power output from the thermal generators. The iteration number was selected to achieve good performance for the suggested GTO technique.

The selection of the controlling parameter of the GTO method was such as any meta-heuristic optimization technique. The trial-and-error method was used to choose these parameters with many independent trials and finally to check the algorithm's performance. Many various cases have been shown to demonstrate the efficacy of the proposed algorithm. All scenarios were ran for fixed and variable loads. The fixed load is the standard load for the standard test systems mentioned in this paper. The variable load is the load of an available summer weekday and is presented in [62]. Figures 10 and 11 show an example of the variable load curve over a summer day at bus 15 for the IEEE 30-bus and IEEE 118 systems, respectively. To prove the efficacy of the proposed approach for OPF and POPF problems, three different scenarios were considered, as are shown in Table 4. The performance and efficacy of the proposed GTO algorithm have been confirmed by comparison with the other chosen approaches.

Table 3. Key features of the three studied systems.

Characteristics	**30-Bus Test System**		**118-Bus Test System**	
	Value	**Detail**	**Value**	**Detail**
Number of buses	30-bus	[43]	118-bus	[63]
Generators	6	Buses-location: 1, 2, 5, 8, 11 and 13	54	Buses-location: 1, 4, 6, 8, 10, 12, 15, 18, 19, 24, 25, 26, 27, 31, 32, 34, 36,40, 42, 46, 49, 54, 55, 56, 59, 61, 62, 65, 66, 69, 70, 72, 73, 74, 76,77, 80, 85, 87, 89, 90, 91, 92, 99, 100, 103, 104, 105, 107, 110,111, 112, 113 and 116
Branches	41		186	
Transformers	4	Branches: 11, 12, 15 and 36	9	Branches: 8, 32, 36, 51, 93, 95, 102, 107 and 127
Loads	21		99	
Connected load (MVA)	283.4 + j126.2		4242 + j1438	
Load losses (MVA)	5.28 + j23.14		132.86 + j783.79	
Bus voltage limits	[0.9–1.1]		[0.9–1.1]	

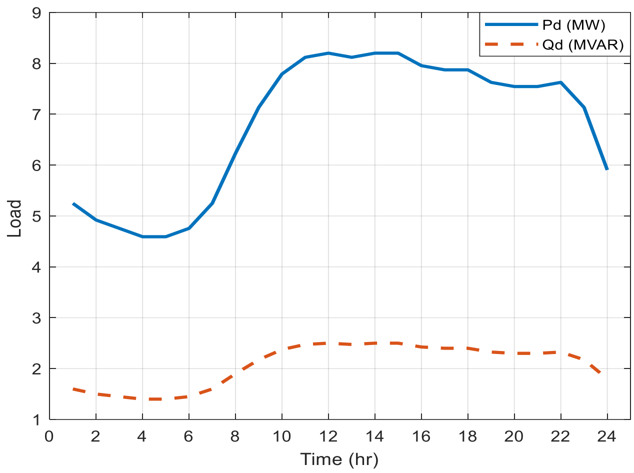

Figure 10. Example of variable load curve for the 30-bus system at bus 15.

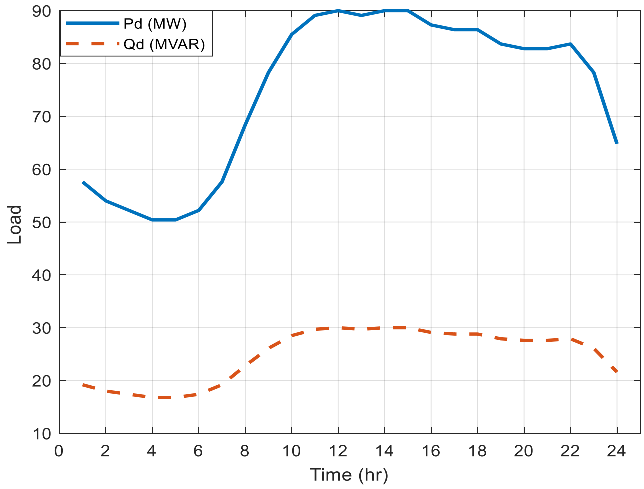

Figure 11. Example of variable load curve for the 118-bus system at bus 15.

Table 4. Scenarios of the OPF.

Scenario No.	The Scenario Details
1	Solve the classical OPF (with no RESs) for fixed loads and compare the results of the proposed technique with the other chosen approaches.
2	Add the PV & Wind generators at the optimal bus location, solve the POPF, and compare the result of the proposed algorithm with other algorithms using fixed and variable loads.
3	Show the effect of adding the PV & wind generators on the total fuel cost using the proposed algorithm with fixed and variable loads.

6.1. The IEEE 30-Bus System

The small-scale power system was used to verify the proposed algorithm's performance. The classical OPF problem with no RESs and the POPF with PV & wind generators at the optimal bus locations were solved. The results were compared to those from other algorithms reported in this paper to confirm their viability. Finally, the proposed algorithm was used to investigate how adding PV and wind generators would affect the system's overall operating costs.

6.1.1. Case 1: Classical OPF

In this case, the proposed technique was used for solving the classical OPF with the fixed load. Its results were then compared to the GA, PSO, SFO, HHO, and HFPSO to verify the performance of the suggested technique. The objective function was to reduce the thermal generator's cost function with no renewable energy added to the system. For all algorithms, the sizes of the population were set at 30. The number of iterations for all algorithms was set at 2000. The optimized control variables and the objective function calculated by GTO are compared to the results from other algorithms in Table 5. Figure 12 shows a comparison of the conversion curve of the objective function for the different algorithms. It is clear from Figure 12 that the GTO outperforms the other techniques in finding the minimum cost with fewer iterations.

Table 5. Comparison of GTO with different algorithms case 1.

	GTO	GA	PSO	SFO	HHO	HFPSO
P_{G1}(MW)	197.2527	194.4922	197.2210	195.7589	196.624	197.2172
P_{G2}(MW)	44.79628	36.03198	44.6978	39.74899	42.11522	44.68869
P_{G3}(MW)	20.4345	21.08808	20.4191	20.74845	21.46444	20.41206
P_{G4}(MW)	10.00067	12.33066	10.1388	13.42112	12.00587	10.15811
P_{G5}(MW)	10	13.85565	10	11.96257	10.01774	10
P_{G6}(MW)	12	16.10798	12	12.48151	12.05558	12
Min Cost($/hr)	915.78184	918.96676	915.78142	916.5774	915.96791	915.78142

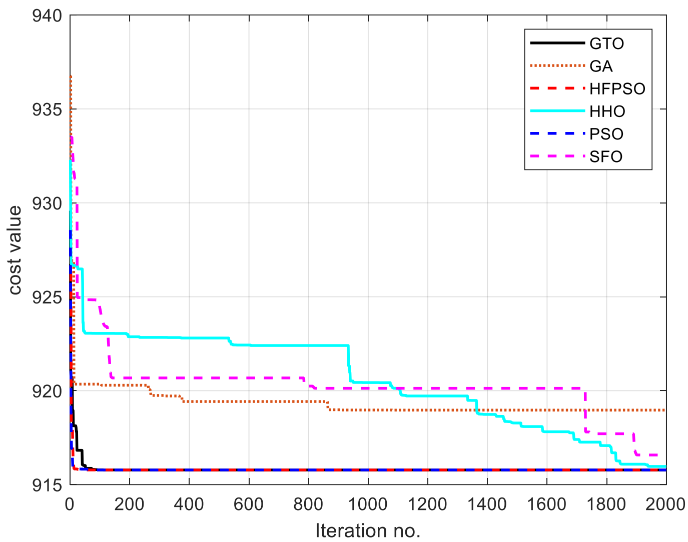

Figure 12. Convergence curve of the objective function using the GTO vs. different algorithms for a 30-bus system.

6.1.2. Case 2: POPF with RESs

In this case, the PV and wind generators were inserted into the optimal bus locations [64], as is shown in Table 6. The rating of the added PV and wind generators were 20 MW and 30 MW, respectively, and were selected such that the total capacity of the RESs represented 17.6% of the total load of the IEEE 30-bus systems. The sizes of the population for all algorithms were set as 15. The number of iterations for all algorithms was set at 200. The proposed technique was used for solving the POPF for fixed and variable loads. The suggested approach's results were then compared to the other chosen algorithms such as the PSO and HHO. The time-varying load is shown in Figure 10 for the standard 30-bus system. Due to changes in irradiance and wind speed, the active power production from the wind and PV generators varied. Therefore, the RESs' uncertainty was considered when forecasting the RESs' output power. Figures 13 and 14 show the convergence of the objective function for the proposed GTO algorithm against the HHO and PSO techniques under fixed and variable loading, respectively. The results indicated that the fuel cost calculated by the GTO is relatively less than the other two algorithms for fixed and variable loads. The results from the proposed approach are significantly superior to results from the other algorithms for fixed load, but for a variable load the results are very similar.

Table 6. Optimal bus location for the RES for different test systems.

	IEEE 30-Bus	IEEE 118-Bus
Optimal bus for PV	4	114
Optimal bus for Wind	21	15

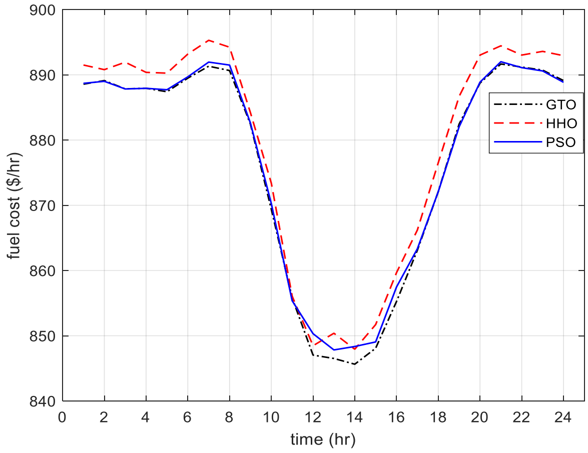

Figure 13. Fuel cost calculated using different algorithms for a fixed load for the 30 bus system.

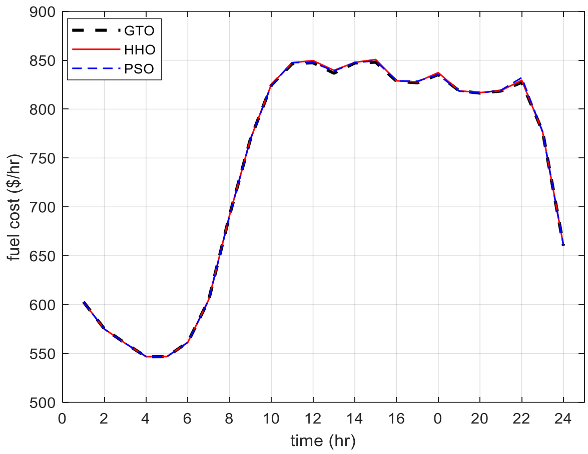

Figure 14. Fuel cost calculated using different algorithms for variable load for the 30 bus system.

6.1.3. Case 3: Effects of Adding the RES on the Total Cost

After confirming that the suggested algorithm successfully founds the optimal results for either the classical OPF or the POPF, the effect of adding the RESs on the system's total operating cost was considered. The proposed algorithm was used for solving the POPF problem considering the uncertainties of the RESs for fixed and time-varying loads. The ratings of the PV, rating of the wind generators, population size, and the number of iterations were kept the same as in the previous case study. Figures 15 and 16 show the effect of adding the RESs to the optimal bus locations on the system's total operating cost. For the fixed and variable loads, adding the PV generators to the system reduced the total cost from hour 7 to hour 20 (as the solar irradiance existed only during this period), while adding the wind generators reduced the total cost throughout the day. Extreme cost reduction occurred when adding both PV and wind generators simultaneously. Tables 7 and 8 summarize the cost reduction percentage from adding PV and wind generators for each hour during the equivalent summer day with fixed and time variable loads, respectively.

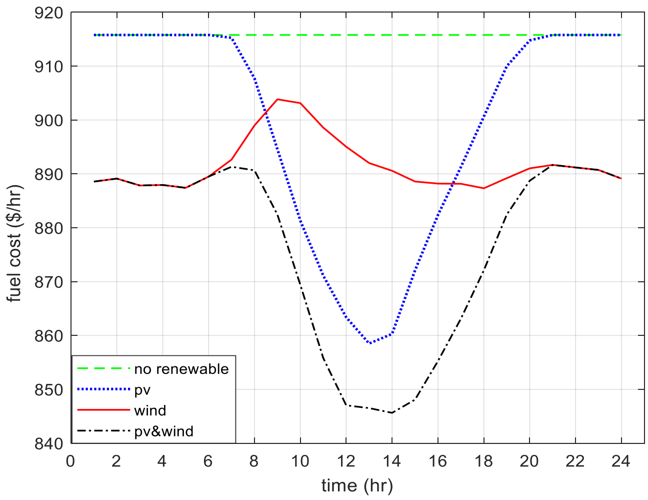

Figure 15. Effect of adding the RES on the total cost for fixed loads for the 30 bus system.

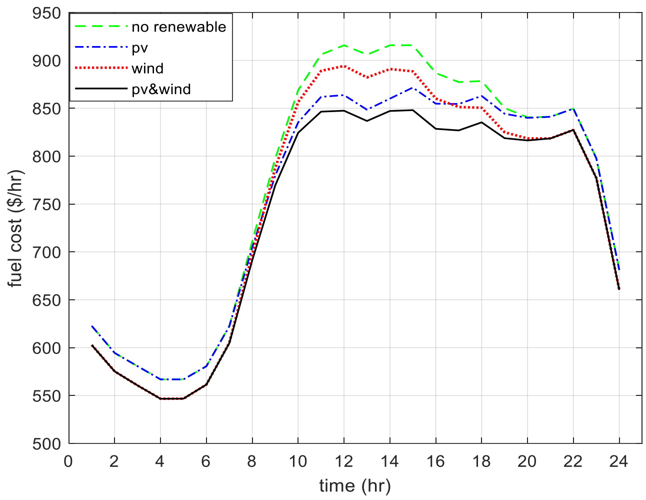

Figure 16. Effect of adding the RES on the total cost for time-varying loads for the 30 bus system.

Table 7. Cost Reduction Percentages resulting from adding PV and wind generators for a fixed load for the 30 bus system.

Hour	**1**	**2**	**3**	**4**	**5**	**6**	**7**	**8**	**9**	**10**	**11**	**12**
PV	0.00%	0.00%	0.00%	0.00%	0.00%	0.00%	0.06%	0.88%	2.31%	3.76%	4.88%	5.72%
Wind	2.97%	2.91%	3.05%	3.04%	3.10%	2.87%	2.53%	1.83%	1.30%	1.38%	1.88%	2.27%
PV & Wind	2.97%	2.91%	3.05%	3.04%	3.10%	2.87%	2.67%	2.74%	3.64%	5.06%	6.55%	7.51%
Hour	**13**	**14**	**15**	**16**	**17**	**18**	**19**	**20**	**21**	**22**	**23**	**24**
PV	6.25%	6.06%	4.77%	3.65%	2.68%	1.65%	0.63%	0.11%	0.00%	0.00%	0.00%	0.00%
Wind	2.60%	2.75%	2.97%	3.01%	3.02%	3.11%	2.90%	2.70%	2.63%	2.69%	2.74%	2.91%
PV & Wind	7.56%	7.66%	7.39%	6.61%	5.75%	4.77%	3.64%	2.95%	2.63%	2.69%	2.74%	2.91%

Table 8. Cost Reduction Percentages resulting from adding PV and wind generators for a variable load for the 30 bus system.

Hour	**1**	**2**	**3**	**4**	**5**	**6**	**7**	**8**	**9**	**10**	**11**	**12**
PV	0.00%	0.00%	0.00%	0.00%	0.00%	0.00%	0.06%	0.90%	2.26%	3.87%	4.88%	5.68%
Wind	3.20%	3.24%	3.46%	3.57%	3.55%	3.30%	2.81%	1.90%	1.26%	1.43%	1.88%	2.36%
PV & W	3.20%	3.24%	3.46%	3.57%	3.55%	3.30%	2.89%	2.78%	3.55%	5.12%	6.58%	7.46%
Hour	**13**	**14**	**15**	**16**	**17**	**18**	**19**	**20**	**21**	**22**	**23**	**24**
PV	6.35%	6.09%	4.82%	3.60%	2.60%	1.78%	0.70%	0.07%	0.00%	0.00%	0.00%	0.00%
Wind	2.62%	2.72%	2.98%	3.00%	2.96%	3.18%	2.98%	2.62%	2.68%	2.61%	2.58%	3.05%
PV & Wind	7.64%	7.49%	7.40%	6.56%	5.75%	4.91%	3.70%	2.88%	2.68%	2.61%	2.58%	3.05%

6.2. The IEEE 118-Bus System

The proposed algorithm's performance was evaluated using the large-scale power system. The classical OPF with no RESs and the POPF with PV and wind generators at the optimal bus locations were solved. The results of the suggested approach were compared with those of the other selected algorithms to confirm its viability. Then, the proposed algorithm was used to study the effect of inserting the PV and wind generators on the system's total operating cost.

6.2.1. Case 4: Classical OPF

The proposed approach was used for solving the classical OPF with the fixed load and then comparing its results with the GA, PSO, SFO, HHO, and HFPSO methods to verify the effectiveness of the suggested technique. The objective function was to reduce the thermal generator's cost function with no renewable energy added to the system. The sizes of the population for all algorithms were set at 30. The number of iterations in all algorithms was set as 2000. The best results of the control variables and the objective function calculated by GTO are compared to the results from other algorithms in Table 9. Figure 17 compares the conversion curve of the objective function for the different algorithms. Comparing other algorithms verified that the GTO algorithm is capable of finding a more advantageous solution.

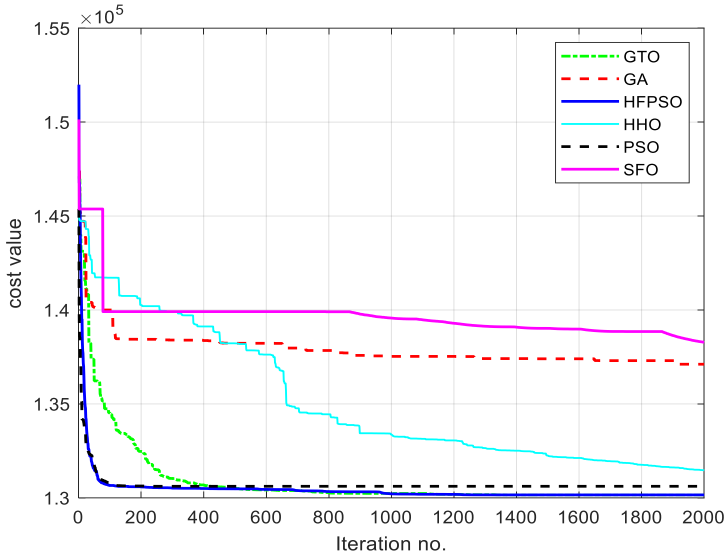

Figure 17. Convergence curve of the objective function using the GTO vs. different algorithms for the 118-bus system.

Table 9. Comparison of the GTO with different algorithms, Case 4.

	GTO	GA	PSO	SFO	HHO	HFPSO
P_{G1}(MW)	26.18848	38.69563	0	80.80498	33.55546	25.46572
P_{G2}(MW)	0	34.54459	0	37.35566	13.1234	0
P_{G3}(MW)	3.131875	40.67364	0	10.77051	5.962829	2.065198
P_{G4}(MW)	0	44.69058	0	46.4833	17.85259	0
P_{G5}(MW)	401.3321	243.0178	415.8368	210.9861	396.2438	400.7185
P_{G6}(MW)	86.44421	79.98373	89.90279	38.33848	95.7612	86.33017
P_{G7}(MW)	25.05885	51.9427	55.35771	22.21952	1.623387	22.81037
P_{G8}(MW)	0	40.09035	0	16.52578	3.903755	14.5435
P_{G9}(MW)	25.13821	48.08774	0	37.95764	3.134425	21.63433
P_{G10}(MW)	2.65×10^{-8}	30.05467	0	62.26664	17.82799	0
P_{G11}(MW)	193.7335	139.6534	200.6964	137.652	140.3687	193.4682
P_{G12}(MW)	279.574	168.6507	289.5222	167.6169	309.3616	279.1499
P_{G13}(MW)	11.16098	37.95601	0	53.09325	16.51134	10.41423
P_{G14}(MW)	7.299935	20.56223	7.614375	25.17363	8.764279	7.290661
P_{G15}(MW)	15.5625	38.14864	0	47.90474	28.8523	14.68148
P_{G16}(MW)	7.759906	44.63419	36.1037	47.32149	30.804	6.87235
P_{G17}(MW)	13.24058	45.07933	37.29125	69.93029	28.07977	12.45803
P_{G18}(MW)	52.0967	38.98866	0	71.70347	10.77414	51.73578
P_{G19}(MW)	45.6204	43.32827	0	82.64717	19.30909	45.43208
P_{G20}(MW)	19.15219	34.06854	19.83277	47.94304	23.70269	19.14443
P_{G21}(MW)	194.3681	123.5074	201.957	220.9543	205.6901	194.3044
P_{G22}(MW)	49.5984	58.71383	51.21706	43.58349	29.95601	49.59079
P_{G23}(MW)	32.61312	41.37444	61.36237	34.85694	3.591768	32.43649
P_{G24}(MW)	33.40108	51.23699	0	63.35362	6.230911	33.22536
P_{G25}(MW)	149.9672	107.3912	153.9797	82.20485	168.4252	149.9155
P_{G26}(MW)	148.3587	111.358	152.3196	111.5377	162.9175	148.2991
P_{G27}(MW)	0	43.39223	0	74.01292	0.802241	0
P_{G28}(MW)	352.8442	257.211	362.4883	181.7175	319.5687	352.6833
P_{G29}(MW)	350.0555	232.6245	360.3861	153.2511	264.4179	349.9061
P_{G30}(MW)	454.4951	335.8225	466.4657	364.7503	458.2573	454.3115
P_{G31}(MW)	0	39.08945	0	59.05702	35.49517	0
P_{G32}(MW)	0	43.71411	6.913055	23.68731	3.786613	0
P_{G33}(MW)	0	42.80282	11.90306	55.47009	17.88553	0
P_{G34}(MW)	15.90603	48.36927	0	22.81919	1.576059	15.61905
P_{G35}(MW)	19.08924	46.80627	0	67.17789	14.88727	18.93601
P_{G36}(MW)	0	44.07293	0	19.75745	16.67851	0
P_{G37}(MW)	432.5556	284.9051	441.0368	340.4575	413.9175	432.4178
P_{G38}(MW)	0	42.07106	0	36.19369	1.307114	0
P_{G39}(MW)	3.622698	16.80306	0	15.01034	1.998334	3.620793
P_{G40}(MW)	495.5841	311.9643	497.4787	320.7231	547.9216	495.508
P_{G41}(MW)	0	52.28653	0	41.33231	33.26819	0
P_{G42}(MW)	0	47.19072	0	55.13177	1.373383	0
P_{G43}(MW)	0	53.90083	0	55.04574	26.08328	0
P_{G44}(MW)	0	44.12449	0	54.94354	3.808979	0
P_{G45}(MW)	231.3747	131.5375	229.8034	192.9504	228.3779	231.3408
P_{G46}(MW)	38.39065	44.31912	37.40516	49.8089	40.07927	38.3863
P_{G47}(MW)	0	47.68645	0	6.309235	10.27407	0
P_{G48}(MW)	4.353593	42.00289	0	64.33285	1.172926	4.309747
P_{G49}(MW)	29.49593	47.15439	21.05478	33.54225	1.518659	29.46746
P_{G50}(MW)	6.676168	48.76126	100	18.5602	47.12069	6.644204
P_{G51}(MW)	35.074	54.01312	32.26676	30.65004	19.77206	35.07286
P_{G52}(MW)	40.89573	57.99037	3.087442	26.42687	29.11091	40.8769
P_{G53}(MW)	0	35.42681	0	41.83573	3.117257	0
P_{G54}(MW)	0	53.13364	0	24.85332	18.9848	0
Min Cost($/hr)	130,159.80628	137,112.90305	130,615.18496	138,281.50269	131,470.33551	130,156.68222

6.2.2. Case 5: POPF with RESs

In this case, the PV and wind generators were inserted into the optimal bus locations [64], as is shown in Table 6. The rating of the added PV and wind generators were 250 MW and 500 MW, respectively. The total capacity of the RESs represents 17.6% of the total system load, such that the percentage of penetration of the RESs was kept the same for the standard 30-bus and 118-bus systems. The sizes of the population for all algorithms were set at 30. The number of iterations for all algorithms was set at 400. The proposed approach was used to solve the POPF, including the RESs, to minimize the fuel cost for fixed and variable loads and to compare the suggested approach with the other chosen algorithms, such as PSO and HHO. The time-varying load is shown in Figure 11 for the standard 118-bus system. Figures 18 and 19 show the convergence curves of the objective function under fixed and variable loading, respectively. The results indicated that the fuel cost calculated by the GTO was less than the other two algorithms for fixed and variable loads, respectively. The results from the proposed approach were significantly superior to results from the other chosen algorithms mentioned in the literature for both fixed and variable loading conditions.

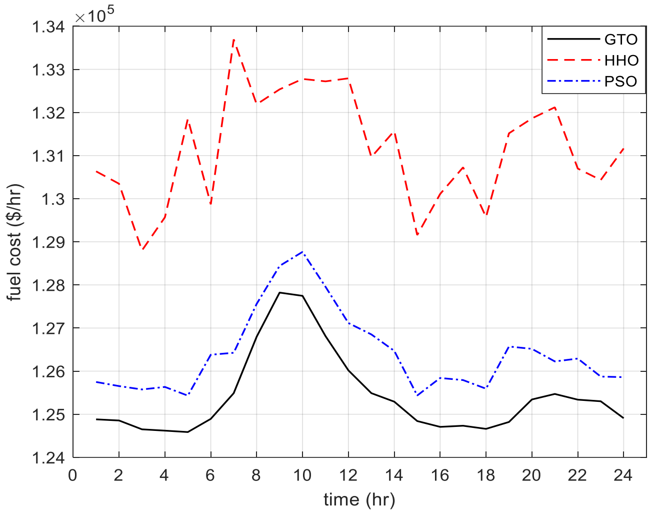

Figure 18. Fuel cost calculated using different algorithms for a fixed load for the 118 bus system.

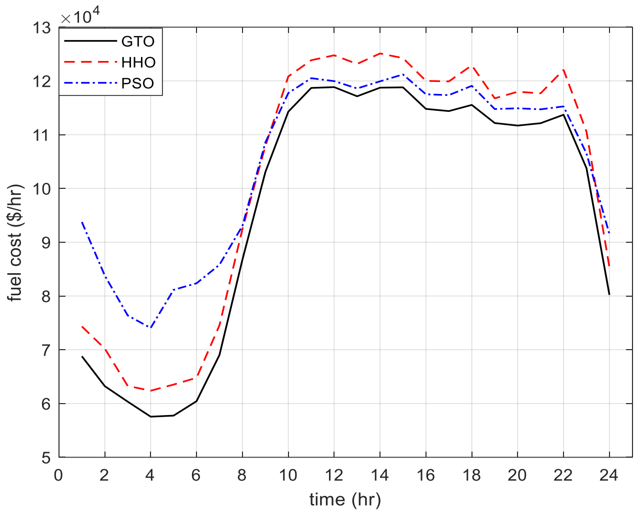

Figure 19. Fuel cost calculated using different algorithms for a variable load for the 118 bus system.

6.2.3. Case 6: Effects of Adding RESs on the Total Cost

After confirming the performance of the suggested approach in finding the optimal solution, whether for classical OPF or POPF in the large-scale system, the effect of adding the RESs on the overall system cost was considered. The proposed approach was used for solving the POPF problem considering the uncertainties of the RESs for fixed and time-varying loads. The ratings of PV generators, wind generators, the size of the population, and the number of iterations were kept the same as in the previous case studies. Figures 20 and 21 show how adding the RESs to the optimal bus locations affects the overall system cost. For the fixed and variable loads, adding the PV generators to the system reduces the total cost from hour 7 to hour 20, as solar irradiance exists only during this period. Adding the wind generators reduces the total cost all over the day, and extreme cost reduction occurs when adding both PV and wind generators simultaneously. Tables 10 and 11 show the cost reduction percentages from adding PV and wind generators for each hour during the equivalent summer day with fixed and variable time loads, respectively. The percentage reduction can be higher for higher RES penetration levels. These reductions happened when only 17.6% of DGs were inserted.

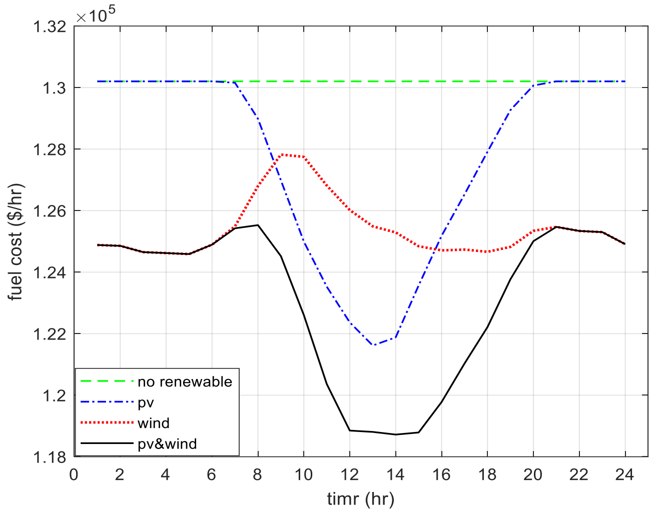

Figure 20. Effect of adding the RESs on the total cost of the IEEE 118-bus system for fixed loads.

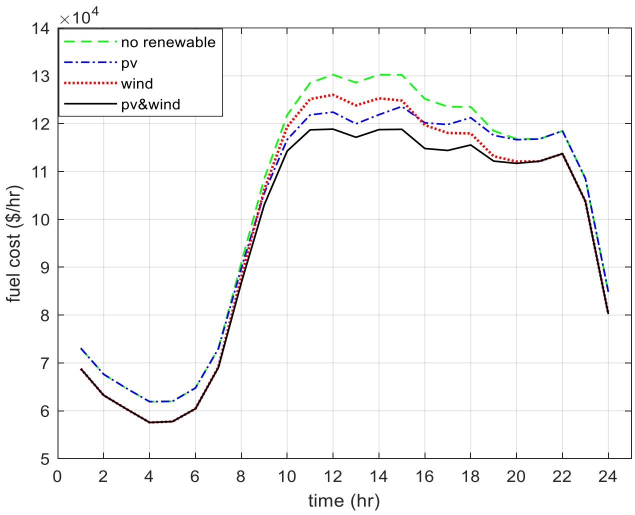

Figure 21. Effect of adding the RESs on the total cost of the IEEE 118-bus system for variableloads.

Table 10. Cost Reduction Percentages resulting from adding PV and wind generators for a fixed load of the 118 bus system.

Hour	1	2	3	4	5	6	7	8	9	10	11	12
PV	0.00%	0.00%	0.00%	0.00%	0.00%	0.00%	0.04%	0.93%	2.47%	4.00%	5.13%	6.02%
Wind	4.09%	4.11%	4.26%	4.29%	4.31%	4.08%	3.62%	2.61%	1.83%	1.89%	2.60%	3.21%
PV & Wind	4.09%	4.11%	4.26%	4.29%	4.31%	4.08%	3.67%	3.59%	4.36%	5.84%	7.56%	8.72%
Hour	**13**	**14**	**15**	**16**	**17**	**18**	**19**	**20**	**21**	**22**	**23**	**24**
PV	6.59%	6.39%	5.10%	3.86%	2.82%	1.76%	0.72%	0.10%	0.00%	0.00%	0.00%	0.00%
Wind	3.62%	3.77%	4.12%	4.22%	4.20%	4.26%	4.13%	3.73%	3.63%	3.74%	3.76%	4.07%
PV & Wind	8.75%	8.82%	8.77%	8.01%	7.04%	6.13%	4.94%	3.99%	3.63%	3.74%	3.76%	4.07%

Table 11. Cost Reduction Percentages resulting from adding PV and wind generators for a variable load of the 118 bus system.

Hour	1	2	3	4	5	6	7	8	9	10	11	12
PV	0.00%	0.00%	0.00%	0.00%	0.00%	0.00%	0.10%	1.21%	2.80%	4.21%	5.20%	6.01%
Wind	5.86%	6.49%	6.69%	7.03%	6.82%	6.69%	5.33%	3.26%	2.11%	2.00%	2.63%	3.23%
PV & Wind	5.86%	6.49%	6.69%	7.03%	6.82%	6.69%	5.48%	4.57%	5.04%	6.17%	7.64%	8.74%
Hour	**13**	**14**	**15**	**16**	**17**	**18**	**19**	**20**	**21**	**22**	**23**	**24**
PV	6.69%	6.43%	5.07%	4.00%	3.03%	1.83%	0.81%	0.15%	0.00%	0.00%	0.00%	0.00%
Wind	3.70%	3.81%	4.13%	4.38%	4.45%	4.48%	4.49%	4.06%	3.98%	4.02%	4.40%	5.46%
PV & Wind	8.88%	8.82%	8.74%	8.29%	7.41%	6.45%	5.35%	4.38%	3.98%	4.02%	4.40%	5.46%

7. Conclusions

In this study, a classical and a probabilistic OPF issue were developed and solved for a hybrid power system that included PV and WE sources with fixed and variable loads. The proposed algorithm was intended to minimize the operational cost of a complex power system. To deal with the uncertainty of the RESs and solve the POPF problem, curve fitting was used for the historical data, applying the most suitable PDFs representing these data. The MCS was then run with many scenarios in combination with the K-means clustering method that minimized the significant computational time. Finally, the optimal number of clusters was calculated using the Elbow approach.

The classical OPF and the POPF problems were solved using the GTO approach. The proposed method was successfully used with different combinations of wind power generation units and solar power generation units in the IEEE 30-bus and 118-bus systems. The performance and efficacy of the proposed algorithm for producing a set of optimal solutions have been proven by comparing the results acquired by the suggested approach with the other optimization techniques. The results of the POPF problem show that inserting the RESs into the system has a significant reduction in the total generation cost. The percentage reduction can be higher for higher RES penetration levels. These reductions happened as only 17% of DGs were inserted. This is essential for the planning and operating of modern power systems that incorporate many alternate forms of energy. Future work will extend our POPF problem to include the cost of renewable energy.

Author Contributions: M.S.H., A.O.B. and H.M.H.: conceptualization and methodology; H.J., A.A. and M.A.: validation, formal analysis; T.A.: investigation, visualization; R.A.T. and F.J.: review and editing. All authors have read and agreed to the published version of the manuscript.

Funding: This work was supported by King Saud University, Riyadh, Saudi Arabia.

Institutional Review Board Statement: Not applicable.

Informed Consent Statement: Not applicable.

Acknowledgments: This work was supported by the Researchers Supporting Project number (RSP2023R467), King Saud University, Riyadh, Saudi Arabia.

Conflicts of Interest: The authors declare no conflict of interest.

References

1. Sun, D.I.; Ashley, B.; Brewer, B.; Hughes, A.; Tinney, W.F. Optimal Power Flow by Newton Approach. *IEEE Trans. Power Appar. Syst.* **1984**, *PAS-103*, 2864–2880. [CrossRef]
2. Lee, K.Y.; Park, Y.M.; Ortiz, J.L. A United Approach to Optimal Real and Reactive Power Dispatch. *IEEE Trans. Power Appar. Syst.* **1985**, *PAS-104*, 1147–1153. [CrossRef]
3. Alsaç, O.; Bright, J.; Prais, M.; Stott, B. Further Developments in Lp-Based Optimal Power Flow. *IEEE Trans. Power Syst.* **1990**, *5*, 697–711. [CrossRef]
4. Monoh, J.A.; Ei-Hawary, M.E.; Adapa, R. A Review of Selected Optimal Power Flow Literature to 1993. II. Newton, Linear Programming and Interior Point Methods. *IEEE Trans. Power Syst.* **1999**, *14*, 105–111. [CrossRef]
5. Momoh, J.A.; Koessler, R.J.; Bond, M.S.; Stott, B.; Sun, D.; Papalexopoulos, A.; Ristanovic, P. Challenges to Optimal Power Flow. *IEEE Trans. Power Syst.* **1997**, *12*, 444–447. [CrossRef]
6. Abido, M.A. Optimal Power Flow Using Particle Swarm Optimization. *Int. J. Electr. Power Energy Syst.* **2002**, *24*, 563–571. [CrossRef]
7. Choudhury, D.; Patra, S. Multi Objective Optimal Power Flow Using Particle Swarm Optimization Technique. In Proceedings of the 2016 International Conference on Signal Processing, Communication, Power and Embedded System (SCOPES), Paralakhemundi, India, 3–5 October 2016; pp. 1261–1266. [CrossRef]
8. Bakirtzis, A.G.; Biskas, P.N.; Zoumas, C.E.; Petridis, V. Optimal Power Flow by Enhanced Genetic Algorithm. *IEEE Trans. Power Syst.* **2002**, *17*, 229–236. [CrossRef]
9. Optimal Power Flow Based on Linear Adapted Genetic Algorithm | Proceedings of the 9th WSEAS International Conference on Applications of Electrical Engineering. Available online: https://dl.acm.org/doi/abs/10.5555/1844259.1844291 (accessed on 18 September 2022).
10. Shaheen, A.M.; El-Sehiemy, R.A.; Farrag, S.M. Solving Multi-Objective Optimal Power Flow Problem via Forced Initialised Differential Evolution Algorithm. *IET Gener. Transm. Distrib.* **2016**, *10*, 1634–1647. [CrossRef]
11. Varadarajan, M.; Swarup, K.S. Solving Multi-Objective Optimal Power Flow Using Differential Evolution. *IET Gener. Transm. Distrib.* **2008**, *2*, 720–730. [CrossRef]
12. Duman, S.; Güvenç, U.; Sönmez, Y.; Yörükeren, N. Optimal Power Flow Using Gravitational Search Algorithm. *Energy Convers. Manag.* **2012**, *59*, 86–95. [CrossRef]
13. Jahan, M.S.; Amjady, N. Solution of Large-Scale Security Constrained Optimal Power Flow by a New Bi-Level Optimisation Approach Based on Enhanced Gravitational Search Algorithm. *IET Gener. Transm. Distrib.* **2013**, *7*, 1481–1491. [CrossRef]
14. Bouchekara, H.R.E.H.; Chaib, A.E.; Abido, M.A.; El-Sehiemy, R.A. Optimal Power Flow Using an Improved Colliding Bodies Optimization Algorithm. *Appl. Soft Comput.* **2016**, *42*, 119–131. [CrossRef]
15. El-Sehiemy, R.A.; Shafiq, M.B.; Azmy, A.M. Multi-Phase Search Optimisation Algorithm for Constrained Optimal Power Flow Problem. *Int. J. Bio-Inspired Comput.* **2014**, *6*, 275–289. [CrossRef]
16. Pulluri, H.; Naresh, R.; Sharma, V. A Solution Network Based on Stud Krill Herd Algorithm for Optimal Power Flow Problems. *Soft Comput.* **2018**, *22*, 159–176. [CrossRef]
17. Niknam, T.; Narimani, M.R.; Aghaei, J.; Azizipanah-Abarghooee, R. Improved Particle Swarm Optimisation for Multi-Objective Optimal Power Flow Considering the Cost, Loss, Emission and Voltage Stability Index. *IET Gener. Transm. Distrib.* **2012**, *6*, 515–527. [CrossRef]
18. Liang, R.H.; Tsai, S.R.; Chen, Y.T.; Tseng, W.T. Optimal Power Flow by a Fuzzy Based Hybrid Particle Swarm Optimization Approach. *Electr. Power Syst. Res.* **2011**, *81*, 1466–1474. [CrossRef]
19. Bhattacharya, A.; Chattopadhyay, P.K. Application of Biogeography-Based Optimisation to Solve Different Optimal Power Flow Problems. *IET Gener. Transm. Distrib.* **2011**, *5*, 70–80. [CrossRef]
20. Bouchekara, H.R.E.H. Optimal Power Flow Using Black-Hole-Based Optimization Approach. *Appl. Soft Comput.* **2014**, *24*, 879–888. [CrossRef]
21. Sivasubramani, S.; Swarup, K.S. Multi-Objective Harmony Search Algorithm for Optimal Power Flow Problem. *Int. J. Electr. Power Energy Syst.* **2011**, *33*, 745–752. [CrossRef]
22. Optimal Power Flow Based on Imperialist Competitive Algorithm | Request PDF. Available online: https://www.researchgate.net/publication/295654369_Optimal_Power_Flow_Based_on_Imperialist_Competitive_Algorithm (accessed on 18 September 2022).
23. El-Fergany, A.A.; Hasanien, H.M. Single and Multi-Objective Optimal Power Flow Using Grey Wolf Optimizer and Differential Evolution Algorithms. *Electr. Power Compon. Syst.* **2015**, *43*, 1548–1559. [CrossRef]
24. Radosavljević, J.; Klimenta, D.; Jevtić, M.; Arsić, N. Optimal Power Flow Using a Hybrid Optimization Algorithm of Particle Swarm Optimization and Gravitational Search Algorithm. *Electr. Power Compon. Syst.* **2015**, *43*, 1958–1970. [CrossRef]
25. Adaryani, M.R.; Karami, A. Artificial Bee Colony Algorithm for Solving Multi-Objective Optimal Power Flow Problem. *Int. J. Electr. Power Energy Syst.* **2013**, *53*, 219–230. [CrossRef]

26. Morshed, M.J.; Fekih, A. A Fault-Tolerant Control Paradigm for Microgrid-Connected Wind Energy Systems. *IEEE Syst. J.* **2018**, *12*, 360–372. [CrossRef]
27. Morshed, M.J.; Fekih, A. A New Fault Ride-through Control for DFIG-Based Wind Energy Systems. *Electr. Power Syst. Res.* **2017**, *146*, 258–269. [CrossRef]
28. Li, G.; Zhang, R.; Jiang, T.; Chen, H.; Bai, L.; Cui, H.; Li, X. Optimal Dispatch Strategy for Integrated Energy Systems with CCHP and Wind Power. *Appl. Energy* **2017**, *192*, 408–419. [CrossRef]
29. Yu, H.; Rosehart, W.D. An Optimal Power Flow Algorithm to Achieve Robust Operation Considering Load and Renewable Generation Uncertainties. *IEEE Trans. Power Syst.* **2012**, *27*, 1808–1817. [CrossRef]
30. Ye, C.J.; Huang, M.X. Multi-Objective Optimal Power Flow Considering Transient Stability Based on Parallel NSGA-II. *IEEE Trans. Power Syst.* **2015**, *30*, 857–866. [CrossRef]
31. Ramadhani, U.H.; Shepero, M.; Munkhammar, J.; Widén, J.; Etherden, N. Review of Probabilistic Load Flow Approaches for Power Distribution Systems with Photovoltaic Generation and Electric Vehicle Charging. *Int. J. Electr. Power Energy Syst.* **2020**, *120*, 106003. [CrossRef]
32. Prusty, B.R.; Jena, D. A Critical Review on Probabilistic Load Flow Studies in Uncertainty Constrained Power Systems with Photovoltaic Generation and a New Approach. *Renew. Sustain. Energy Rev.* **2017**, *69*, 1286–1302. [CrossRef]
33. Ullah, Z.; Wang, S.; Wu, G.; Hasanien, H.M.; Jabbar, M.W.; Qazi, H.S.; Tostado-Véliz, M.; Turky, R.A.; Elkadeem, M.R. Advanced Studies for Probabilistic Optimal Power Flow in Active Distribution Networks: A Scientometric Review. *IET Gener. Transm. Distrib.* **2022**, *16*, 3579–3604. [CrossRef]
34. Aien, M.; Fotuhi-Firuzabad, M.; Rashidinejad, M. Probabilistic Optimal Power Flow in Correlated Hybrid Wind-Photovoltaic Power Systems. *IEEE Trans. Smart Grid* **2014**, *5*, 130–138. [CrossRef]
35. Ruiz-Rodriguez, F.J.; Hernández, J.C.; Jurado, F. Probabilistic Load Flow for Photovoltaic Distributed Generation Using the Cornish–Fisher Expansion. *Electr. Power Syst. Res.* **2012**, *89*, 129–138. [CrossRef]
36. Morshed, M.J.; Ben Hmida, J.; Fekih, A. A Probabilistic Multi-Objective Approach for Power Flow Optimization in Hybrid Wind-PV-PEV Systems. *Appl. Energy* **2018**, *211*, 1136–1149. [CrossRef]
37. Rahmani, S.; Amjady, N. A New Optimal Power Flow Approach for Wind Energy Integrated Power Systems. *Energy* **2017**, *134*, 349–359. [CrossRef]
38. Cao, J.; Yan, Z. Probabilistic Optimal Power Flow Considering Dependences of Wind Speed among Wind Farms by Pair-Copula Method. *Int. J. Electr. Power Energy Syst.* **2017**, *84*, 296–307. [CrossRef]
39. Chen, J.J.; Wu, Q.H.; Zhang, L.L.; Wu, P.Z. Multi-Objective Mean–Variance–Skewness Model for Nonconvex and Stochastic Optimal Power Flow Considering Wind Power and Load Uncertainties. *Eur. J. Oper. Res.* **2017**, *263*, 719–732. [CrossRef]
40. Zou, B.; Xiao, Q. Solving Probabilistic Optimal Power Flow Problem Using Quasi Monte Carlo Method and Ninth-Order Polynomial Normal Transformation. *IEEE Trans. Power Syst.* **2014**, *29*, 300–306. [CrossRef]
41. Xiao, Q. Comparing Three Methods for Solving Probabilistic Optimal Power Flow. *Electr. Power Syst. Res.* **2015**, *124*, 92–99. [CrossRef]
42. Shargh, S.; Khorshid ghazani, B.; Mohammadi-ivatloo, B.; Seyedi, H.; Abapour, M. Probabilistic Multi-Objective Optimal Power Flow Considering Correlated Wind Power and Load Uncertainties. *Renew. Energy* **2016**, *94*, 10–21. [CrossRef]
43. Ghasemi, M.; Ghavidel, S.; Ghanbarian, M.M.; Gharibzadeh, M.; Azizi Vahed, A. Multi-Objective Optimal Power Flow Considering the Cost, Emission, Voltage Deviation and Power Losses Using Multi-Objective Modified Imperialist Competitive Algorithm. *Energy* **2014**, *78*, 276–289. [CrossRef]
44. Shaheen, M.A.M.; Hasanien, H.M.; Mekhamer, S.F.; Qais, M.H.; Alghuwainem, S.; Ullah, Z.; Tostado-Véliz, M.; Turky, R.A.; Jurado, F.; Elkadeem, M.R. Probabilistic Optimal Power Flow Solution Using a Novel Hybrid Metaheuristic and Machine Learning Algorithm. *Mathematics* **2022**, *10*, 3036. [CrossRef]
45. Jiang, P.; Liu, Z.; Niu, X.; Zhang, L. A Combined Forecasting System Based on Statistical Method, Artificial Neural Networks, and Deep Learning Methods for Short-Term Wind Speed Forecasting. *Energy* **2021**, *217*, 119361. [CrossRef]
46. Reddy, Y.; Jithendranath, J.; Chakraborty, A.K.; Guerrero, J.M. Stochastic Optimal Power Flow in Islanded DC Microgrids with Correlated Load and Solar PV Uncertainties. *Appl. Energy* **2022**, *307*, 118090. [CrossRef]
47. Li, S.; Gong, W.; Wang, L.; Gu, Q. Multi-Objective Optimal Power Flow with Stochastic Wind and Solar Power. *Appl. Soft Comput.* **2022**, *114*, 108045. [CrossRef]
48. Gualtieri, G.; Secci, S. Methods to Extrapolate Wind Resource to the Turbine Hub Height Based on Power Law: A 1-h Wind Speed vs. Weibull Distribution Extrapolation Comparison. *Renew. Energy* **2012**, *43*, 183–200. [CrossRef]
49. Kumari, B.A.; Vaisakh, K. Integration of Solar and Flexible Resources into Expected Security Cost with Dynamic Optimal Power Flow Problem Using a Novel DE Algorithm. *Renew. Energy Focus* **2022**, *42*, 48–69. [CrossRef]
50. Andreas, A.; Stoffel, T. NREL Solar Radiation Research Laboratory (SRRL): Baseline Measurement System (BMS); Golden, Colorado (Data). NREL Report No. DA-5500-56488; 1981. Available online: https://midcdmz.nrel.gov/apps/sitehome.pl?site=BMS#DOI (accessed on 7 September 2022).
51. Kim, S.; Hur, J. A Probabilistic Modeling Based on Monte Carlo Simulation of Wind Powered EV Charging Stations for Steady-States Security Analysis. *Energies* **2020**, *13*, 5260. [CrossRef]
52. Liu, Y.; Guo, L.; Hou, R.; Wang, C.; Wang, X. A Hybrid Stochastic/Robust-Based Multi-Period Investment Planning Model for Island Microgrid. *Int. J. Electr. Power Energy Syst.* **2021**, *130*, 106998. [CrossRef]

53. Syakur, M.A.; Khotimah, B.K.; Rochman, E.M.S.; Satoto, B.D. Integration K-Means Clustering Method and Elbow Method For Identification of The Best Customer Profile Cluster. *IOP Conf. Ser. Mater. Sci. Eng.* **2018**, *336*, 012017. [CrossRef]
54. Umargono, E.; Suseno, J.E.; Gunawan, S.V. K-Means Clustering Optimization Using the Elbow Method and Early Centroid Determination Based on Mean and Median Formula. In Proceedings of the 2nd International Seminar on Science and Technology (ISSTEC 2019), Yogyakarta, Indonesia, 25–26 November 2019; Atlantis Press: Paris, France, 2020. [CrossRef]
55. Liu, L.; Peng, Z.; Wu, H.; Jiao, H.; Yu, Y.; Zhao, J. Fast Identification of Urban Sprawl Based on K-Means Clustering with Population Density and Local Spatial Entropy. *Sustainability* **2018**, *10*, 2683. [CrossRef]
56. Abdollahzadeh, B.; Gharehchopogh, F.S.; Mirjalili, S. Artificial Gorilla Troops Optimizer: A New Nature-Inspired Metaheuristic Algorithm for Global Optimization Problems. *Int. J. Intell. Syst.* **2021**, *36*, 5887–5958. [CrossRef]
57. Osman, M.S.; Abo-Sinna, M.A.; Mousa, A.A. A Solution to the Optimal Power Flow Using Genetic Algorithm. *Appl. Math. Comput.* **2004**, *155*, 391–405. [CrossRef]
58. Turkay, B.E.; Cabadag, R.I. Optimal Power Flow Solution Using Particle Swarm Optimization Algorithm. *IEEE EuroCon 2013* **2013**, 1418–1424. [CrossRef]
59. Shaheen, M.A.M.; Hasanien, H.M.; Mekhamer, S.F.; Talaat, H.E.A. Optimal Power Flow of Power Systems Including Distributed Generation Units Using Sunflower Optimization Algorithm. *IEEE Access* **2019**, *7*, 109289–109300. [CrossRef]
60. Islam, M.Z.; Abdul Wahab, N.I.; Veerasamy, V.; Hizam, H.; Mailah, N.F.; Khan, A.; Sabo, A. Optimal Power Flow Using a Novel Harris Hawk Optimization Algorithm to Minimize Fuel Cost and Power Loss. 2019 IEEE Conf. Sustain. *Util. Dev. Eng. Technol. CSUDET* **2019**, *2019*, 246–250. [CrossRef]
61. Khan, A.; Hizam, H.; bin Abdul Wahab, N.I.; Othman, M.L. Optimal Power Flow Using Hybrid Firefly and Particle Swarm Optimization Algorithm. *PLoS ONE* **2020**, *15*, e0235668. [CrossRef]
62. Grigg, C.; Wong, P. The IEEE Reliability Test System -1996 a Report Prepared by the Reliability Test System Task Force of the Application of Probability Methods Subcommittee. *IEEE Trans. Power Syst.* **1999**, *14*, 1010–1020. [CrossRef]
63. Index of /Data. Available online: http://motor.ece.iit.edu/data/ (accessed on 14 August 2022).
64. Shaheen, M.A.M.; Hasanien, H.M.; Al-Durra, A. Solving of Optimal Power Flow Problem Including Renewable Energy Resources Using HEAP Optimization Algorithm. *IEEE Access* **2021**, *9*, 35846–35863. [CrossRef]